Available online at ScienceDirect

Nuclear Engineering and Technology

journal homepage: www.elsevier.com/locate/net

Original Article

An Assessment of the Secondary Neutron Dose in the Passive Scattering Proton Beam Facility of the National Cancer Center

Sang-Eun Han [a,b,*], *Gyuseong Cho* [b], *and Se Byeong Lee* [c]

[a] *Korea Institute of Nuclear Safety, 34 Gwahak-ro, Yuseong-gu, Daejeon 305-338, South Korea*
[b] *Korea Advanced Institute of Science and Technology, 291 Daehak-ro, Yuseong-gu, Daejeon 305-701, South Korea*
[c] *Proton Therapy Center, National Cancer Center, 323 Ilsan-ro, Ilsan dong-gu, Goyang 410-769, South Korea*

ARTICLE INFO

Article history:
Received 11 August 2016
Received in revised form
10 October 2016
Accepted 5 December 2016
Available online 28 December 2016

Keywords:
MCNP
Neutron Dose Assessment
Proton Therapy
Secondary Neutron

ABSTRACT

The purpose of this study is to assess the additional neutron effective dose during passive scattering proton therapy. Monte Carlo code (Monte Carlo N-Particle 6) simulation was conducted based on a precise modeling of the National Cancer Center's proton therapy facility. A three-dimensional neutron effective dose profile of the interior of the treatment room was acquired via a computer simulation of the 217.8-MeV proton beam. Measurements were taken with a ^{3}He neutron detector to support the simulation results, which were lower than the simulation results by 16% on average. The secondary photon dose was about 0.8% of the neutron dose. The dominant neutron source was deduced based on flux calculation. The secondary neutron effective dose per proton absorbed dose ranged from 4.942 ± 0.031 mSv/Gy at the end of the field to 0.324 ± 0.006 mSv/Gy at 150 cm in axial distance.

1. Introduction

Radiation therapy using heavy charged particles (HCPs) is an advanced technique of delivering energy to the target volume effectively. HCPs lose a small amount of energy at the point of penetration but release most of their energy near the end of the beam path length. This is a property of HCPs that contrasts with that of photons, and this results in less dose to normal tissues surrounding the target volume. Because of this advantageous characteristic, HCP therapy has been researched in many countries, and the number of HCP research facilities has been increasing at a rapid rate. According to the statistics of the Particle Therapy Co-Operation Group, 56 heavy particle therapy facilities are operating in 15 counties as of the end of 2014, and 29 facilities are currently under construction [1].

Proton beams, a common type of HCP used for clinical purposes, can be used to treat tumors located in sensitive organs such as the head, neck, skull base, and brain. These organs are difficult or impossible to treat with photons because of the potential adverse effects on normal cells [2]. With that being said, however, despite the clinical merits of proton beams, there are health risks associated with their use arising from secondary radiations such as photons and neutrons [3, 4].

* *Corresponding author.*
E-mail address: k496hse@kins.re.kr (S.-E. Han).
http://dx.doi.org/10.1016/j.net.2016.12.003

Neutrons, the dominant particles that contribute to the risk, are primarily generated from high-energy proton interactions with structural materials such as the metal part of the beam nozzle and the concrete wall [5]. The proton beams are initially narrow, with a radius of several millimeters at the entrance (start point) of the therapy nozzle. However, they are widened and modified to be made suitable for treatment, which in turn increases the probability of negative interactions. There are two common options for beam modification: one is to use uniform and large field irradiation, and the other is to use small field scanning. The former is defined as passive (or double) scattering [6, 7] and the latter as dynamic scanning [8, 9]. Passive scattering is a process that generates more neutrons owing to the need for more physical components, which widen the irradiated field.

According to previous studies (Table 1), secondary neutron dose varies from 0.1 mSv/Gy to 8 mSv/Gy (mSv/Gy denotes the effective dose per proton absorbed dose in target) under passive scattering conditions. This suggests that the expected additional neutron doses are not negligible, and could constitute a potential health risk. Nevertheless, more data need to be collected because most proton therapy facilities have unique design features and a variety of beam conditions.

In order to assess the secondary neutron effective dose in the treatment area, preparations were made for the Monte Carlo N-Particle 6 (MCNP6) simulation and measurements. The proton beam nozzle was modeled precisely based on a computer-aided design (CAD) drawing; 183,530 points of the treatment room were calculated to obtain a dose profile. The simulation results for the location at which patients are typically positioned were compared to the ^{3}He (helium-3) neutron measurement data. The uncertainty levels of the simulation and of the measurement data were determined at a 95% confidence level. The reference site was the 230-MeV proton therapy facility of the National Cancer Center (NCC), the first of its kind in Korea, which opened in 2007.

2. Materials and methods

2.1. Proton beam nozzle modeling

The MCNP6 (ver. 1.0) [17] radiation transport code was used to simulate the proton beam delivery system and the treatment facility of the NCC. Physics data libraries based on ENDF/B-VII and the Cascade-Exciton Model (CEM03.03) and on the Los Alamos Quark-Gluon String Model (LAQGSM03.03) nuclear interaction physics models were applied for the calculation. Data on the geometry and size were collected from CAD drawings and measurements on site at the NCC. The key components contributing to the neutron field—such as the passive scattering system, range modulator, snout, and shielding walls—were processed with precision, whereas the minor parts were appropriately simplified for calculation efficiency.

Table 1 – Summary of assessment studies of secondary neutron dose in passive scattering proton therapy.

Author	Dosimetry method	Beam energy (MeV)	Neutron dose (mSv/Gy)
Yan et al [10]	Measurement	160	0.1–0.32
Roy and Sandison [11]	Measurement	198	0.1–0.26
Polf and Newhauser [12]	Monte Carlo	158	0.63–6.3
Mesoloras et al [13]	Measurement	134, 119	0.03–0.87
Tayama et al [14]	Measurement	200	2 max
Wroe et al [15]	Measurement	225	3.9–0.18
Zheng et al [16]	Monte Carlo	250	1–8

The proton beam was defined as a type of mono energy, and probability distribution as Gaussian step functions of 0.58, 0.32, 0.09, and 0.01 within a 15-mm radius. The range modulator was composed of 23 steps in a circular track with height ranging from 0 mm to 138.93 mm; the contribution time of each step was determined based on the angular width. The second scatterer, an 8-cm circular disk with a Gaussian-shaped plane, consists of 1-mm-wide circular steps from the center to the outer circumference of the circle.

Fig. 1 shows the nozzle configuration and the proton beam shape. A narrow proton beam generated at the entrance of the nozzle traverses the first scatterer (multilead layer), range modulator wheel (polycarbonate), and the second scatterer (polycarbonate and lead disk). As the beam passes through these components, the beam field widens laterally and the dose gets distributed uniformly along the target depth. A wider beam is processed using the snout (stainless steel and bronze), aperture (bronze), and bolus (polymethyl methacrylate) according to the clinical purpose. Then, finally, the beam reaches the target volume in the water phantom.

2.2. Simulated nozzle performance test

Prior to the main calculation, the proton beam range of the simulated nozzle was compared to the physical data provided by the National Institute of Standards and Technology [18] for performance verification. The water phantom (40 cm × 40 cm × 40 cm) was located in front of the nozzle, and proton beams were generated in the 150 MeV to 230 MeV energy range with a 10-MeV step. In order to obtain a pure beam range, the components on the beam axis line that were traversed by the beam, such as the scatterer, range modulator, and bolus, were not taken into consideration. The actual beam range was acquired at the 10% maximum point [19] on the energy deposition curve. Table 2 shows the results. The two pieces of data matched well over the whole set of energy steps; the maximum difference between two pieces of data was 0.8% at 230 MeV.

2.3. Dose calculation

The proton beam nozzle was located in a treatment room surrounded by concrete (density, 2.3 g/cm^{3}) shields. The water phantom was positioned on the patient bed 3 cm away from the end of the nozzle. The proton beam strength was 217.8 MeV and 7 nA, which is common in clinical settings. The beam opening was 4 cm in radius, and the beam range was 21.25 cm (the range modulation was 5 cm) in water in the passive scattering mode (Fig. 2).

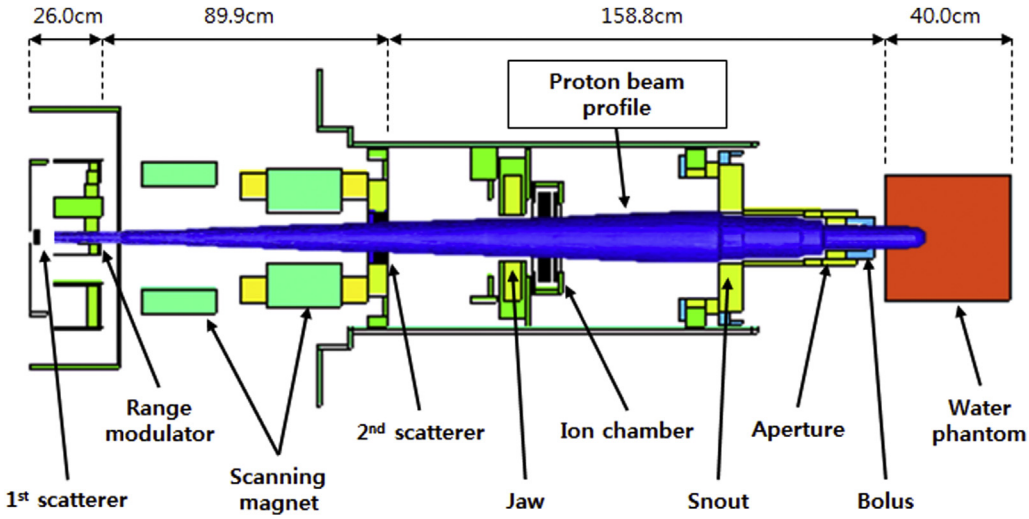

Fig. 1 – Cross-sectional schematic diagram of the proton beam nozzle used at NCC. The proton beam profile image was overlapped on MCNP6 geometry plot. The beam, which is projected from the entrance of the nozzle, expands through the first and second scatterers, is tailored by the snout, aperture and bolus and, finally, is delivered to the target. MCNP6 = Monte Carlo N-Particle 6; NCC = National Cancer Center.

Detectors (calculation points) were arrayed over the whole treatment space including the nozzle, at intervals of 10 cm from the beam entrance, in a three-dimensional (3D) mesh. The origin (0, 0, 0) indicates the entrance of the beam. The Z axis is the proton beam axis, and the X and Y axes are perpendicular to the beam axis (X axis, −800 cm to 850 cm; Y axis, −120 cm to 0 cm; Z axis, −400 cm to 1,150 cm). The detectors collected data on neutron/photon flux, which were then converted to dose using conversion constants ICRP (International Commission on Radiological Protection) 74 [20] for neutrons and photons. ICRP 74 is based on ICRP 60 (1990), and ICRP 60 was revised into ICRP 103 (2007). Even though, based on ICRP 103, changes were made to the neutron dose conversion factors in ICRP 116, ICRP 74 was adopted in this study because the detector was calibrated with ICRP 74.

2.4. Measurements

2.4.1. Instrument

A Wide-Energy Neutron Detector (Thermo Scientific, WENDI-2) was procured. This detector has a higher sensitivity (0.84 cps per μSv/h) than that of common BF-3 type neutron detectors and has a wide energy response range of 25 meV to 5 GeV. There is a ^{3}He proportional counter at the center of a cylindrical polyethylene moderator (22.86 cm diameter × 21 cm length), and a tungsten carbide powder shell is inserted between the probe and moderator in order to improve the high energy response [21]. The detector was calibrated using a ^{252}Cf neutron standard source of the Korea Atomic Energy Research Institute, a laboratory that has been accredited by the Korea Laboratory Accreditation Scheme. The calibration factor was 0.95 with 7.5% uncertainty at the 95% confidence level.

Table 2 – Range in water compared to reference data for proton beams in the range 150 MeV to 230 MeV.

Energy (MeV)	Range (cm)		Difference (%)
	NIST	This study	
150	15.76	15.74	0.1
170	19.59	19.65	−0.3
190	23.74	23.87	−0.5
210	28.19	28.37	−0.6
230	32.91	33.16	−0.8

Difference between the simulated nozzle and NIST data was less than 0.8%.
NIST = National Institute of Standards and Technology.

2.4.2. Setup

Fig. 3 shows the overall measurement scheme. Neutron dose (ambient dose equivalent) measurements with the ^{3}He detector were taken at 9 points near the target, including the patient position.

All points were located on the same plane, parallel to the floor. An 8-cm-diameter aperture and bolus were mounted on the snout, and the water phantom (40 cm × 40 cm × 40 cm) was placed on the patient bed 3 cm away from the end of the bolus. The proton beam energy was 217.8 MeV with a 5-cm range modulation; the current was 7 nA, which was the same condition as that used for the simulation.

3. Results

3.1. Photon contribution

Nuclear interaction between high-energy protons and the nuclei of structural materials generates many types of secondary particles and radiation such as pions, muons, electrons, photons, protons, and neutrons [5]. The total secondary dose is the sum of each contribution. However, because most of the doses come from neutrons and photons, this study estimated photon contribution. Neutron and photon doses at

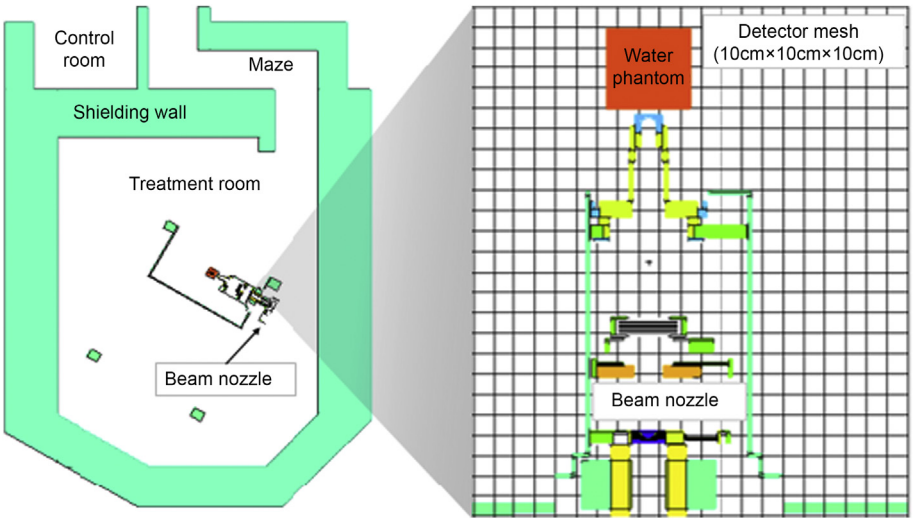

Fig. 2 – Configurations for MCNP6 simulation. The proton beam nozzle was positioned on a plane parallel to the floor in the treatment room (left) and 10-cm mesh detectors were arrayed all over the facility space (right). MCNP6 = Monte Carlo N-Particle 6.

the same position were calculated until 10 statistical parameters passed the MCNP's criteria. Error was determined according to the calculation error of MCNP. The results are compared in Table 3. Photon doses were 0.47% to 1.71% of the neutron doses along the beam axis in the −100 cm to 500 cm range, and the average ratio was 0.8%—that is, photon contribution to the total dose was sufficiently lower than the neutron contribution.

3.2. *Secondary neutron sources*

To verify the contribution of each nozzle component, neutron flux data were acquired along the beam axis. Fig. 4 shows the neutron flux data and a comparison of the physical positions at the nozzle. Notable values were 1.35×10^7 at 10 cm, 2.23×10^7 at 30 cm, 3.49×10^7 at 110 cm, 1.51×10^7 at 230 cm, and 2.63×10^7 at 260 cm from the beam entrance of nozzle (Z = 0 cm) in units of neutrons/cm^2/s. From the above data, we were able to confirm that the dominant neutron sources were the traverse components such as the first scatterer (10 cm), range modulator (30 cm), second scatterer (110 cm), snout (230 cm), and aperture (260 cm).

Fig. 5 shows the neutron energy distribution at the target. The energy scale was the same as the dose conversion factor on ICRP 74. Numerous neutrons were generated at low energy (between 0.01 eV and 200 keV), but this is negligible in terms of the neutron dose because the dose conversion factor is very low at energy levels below 300 keV. The dominant neutron dose originated from the high energy band (between 1 MeV and 100 MeV)

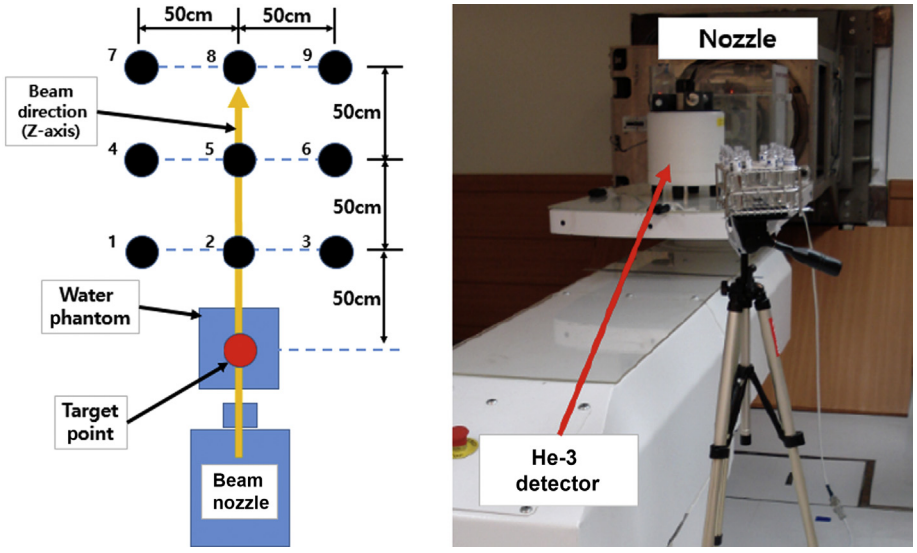

Fig. 3 – Nine points around target were selected for experimental measurements. Points #1 to #9 were selected at intervals of 50 cm along the beam direction (Z axis, colored orange) and these points were laid on the floor parallel plain.

Table 3 – Photon doses compared to neutron doses at the same position as used in the simulation.

Position (Z axis) (cm)	Neutron		Photon		Ratio (B/A) (%)
	Dose (A) (mSv)	Error	Dose (B) (mSv)	Error	
−100	104.06	0.02	0.78	0.03	0.75
0	8,896.46	0.00	41.61	0.00	0.47
100	6,544.75	0.00	31.81	0.00	0.49
200	3,365.64	0.00	27.60	0.00	0.82
300	615.16	0.01	10.54	0.01	1.71
400	73.02	0.02	0.54	0.03	0.74
500	59.17	0.02	0.41	0.04	0.70

Error is the calculation error of Monte Carlo N-Particle (MCNP). The photon/neutron dose ratios are listed as a percentage, with the average of that ratio being 0.8%.

3.3. *Secondary neutron dose in the treatment room*

A 3D neutron and photon dose profile of the treatment room was acquired from the MCNP mesh detector calculation of the 217.8-MeV proton beam. Fig. 6 shows the neutron effective dose profile graphically with a contour line on the beam axis plane. A strong dose field was observed in the beam collision areas such as the first scatterer, range modulator, second scatterer, snout, and aperture. The highest dose was 33.55 Sv/h at the second scatter position, but the neutron dose was observed to decrease rapidly outside of the nozzle. The dose level was about 500 mSv/h near the nozzle surface, 100 mSv/h within 2 m of the nozzle, and between 10 mSv/h and 50 mSv/h in most of the treatment room space. Finally, the neutron field was found to diminish because of the shielding walls and maze structure.

On the basis of the above neutron profile, the neutron effective dose per 1 Gy therapeutic proton absorbed dose at the target was calculated. Table 4 lists the dose distribution near the target position. The highest value was 7.51 mSv/Gy at the target position; the dose decreased to 0.35 mSv/Gy at a lateral distance of 200 cm from the beam axis. Also, a value of 0.31 mSv/Gy was estimated at a position 200 cm distant from the target along the beam axis; the dose decreased to 0.20 mSv/Gy along the lateral distance.

Angular dose dependency was analyzed. Table 5 shows the angular dose equivalent at a constant radius from the target. Values were distributed from 7.12 mSv/Gy (angle, 135°; distance, 50 cm) to 0.33 mSv/Gy (angle, 0°; distance, 150 cm).

More angular dose data were processed graphically as shown in Fig. 7. The neutron dose briefly decreased with increasing distance from the target. The lateral area (about 30° to 150°) had levels higher than those of the front area (about 0° to 30°), whereas the back area (about 150° to 180°) had the highest levels.

In the water phantom (15 cm radius), the dose was constant around the target but increased from 90° to 180° because of the radiation field effect generated by the nozzle. As for the areas outside of the water phantom (50 cm to 150 cm radius), the dose was relatively low in the front area. From this, it was inferred that the field was weakened by the shielding effect of the water phantom. The dose, by contrast, increased rapidly at the backside because of the inclusion of secondary radiation sources of the nozzle, such as the aperture and snout. The dose equivalent distribution ranged from 1.65 mSv/Gy to 18.14 mSv/Gy at 15 cm radius, 0.51 mSv/Gy to 66.35 mSv/Gy at 50 cm

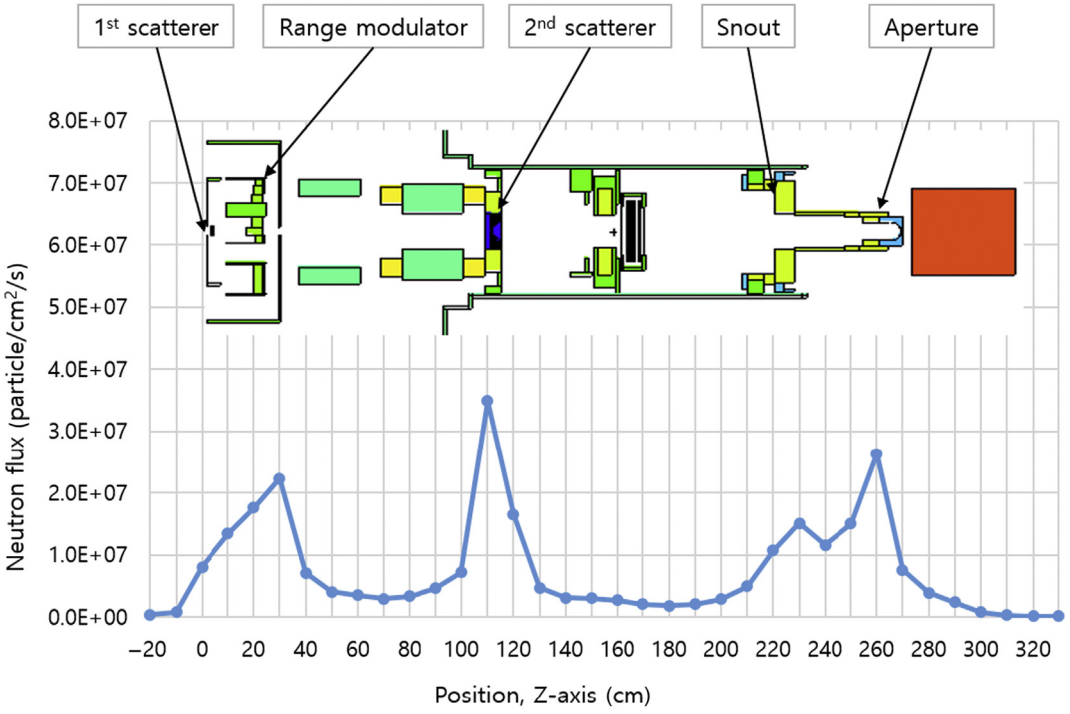

Fig. 4 – Neutron flux distribution along the beam axis (Z axis). The highest value was near the second scatterer; the other dominant sources were the first scatterer, range modulator, snout and aperture.

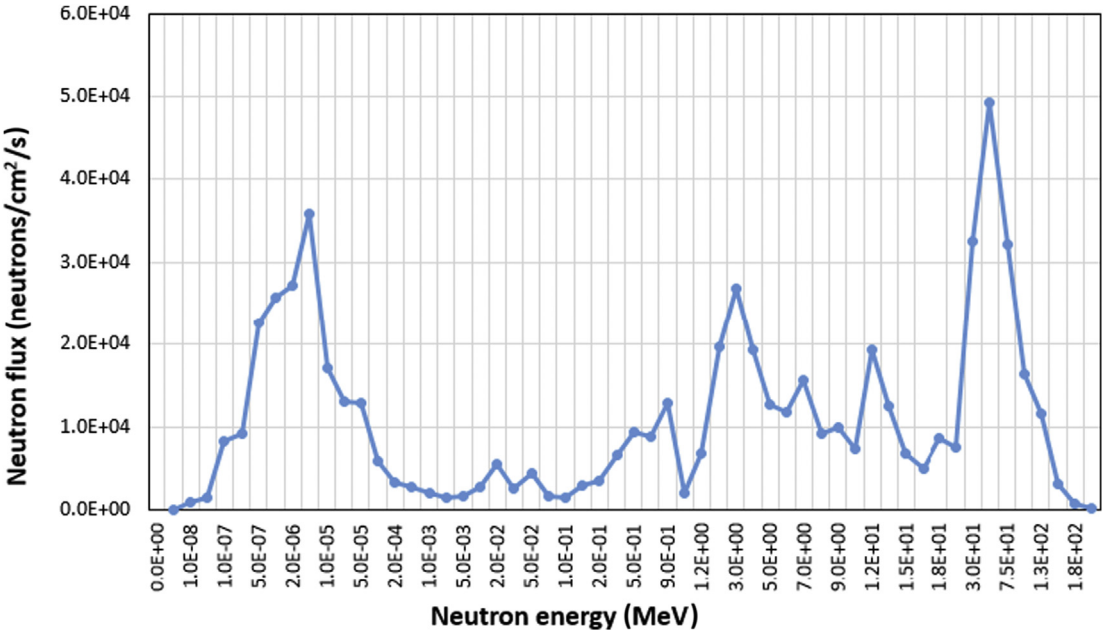

Fig. 5 – Simulated energy distribution of neutron dose flux at target position. High flux was observed at 5 eV, 3 MeV, 12 MeV, and 50 MeV.

radius, 0.38 mSv/Gy to 13.44 mSv/Gy at 100 cm radius, and 0.33 mSv/Gy to 21.14 mSv/Gy at 150 cm radius from the target.

3.4. *Comparison between simulation and measurements*

Fig. 8 provides a comparison between the simulation results and the measurements at the same position, expressed in millisieverts per 1 Gy proton absorbed dose at the target. The measured data showed tendencies similar to those of the simulated data, but the measurements had had values 16% lower than the simulation values, on average. The neutron dose was 0.97 ± 0.01 mSv/Gy (simulation) and 0.78 ± 0.07 mSv/Gy (measurement) at the target nearest position (#3, 50 cm distance along the beam axis from the target), and

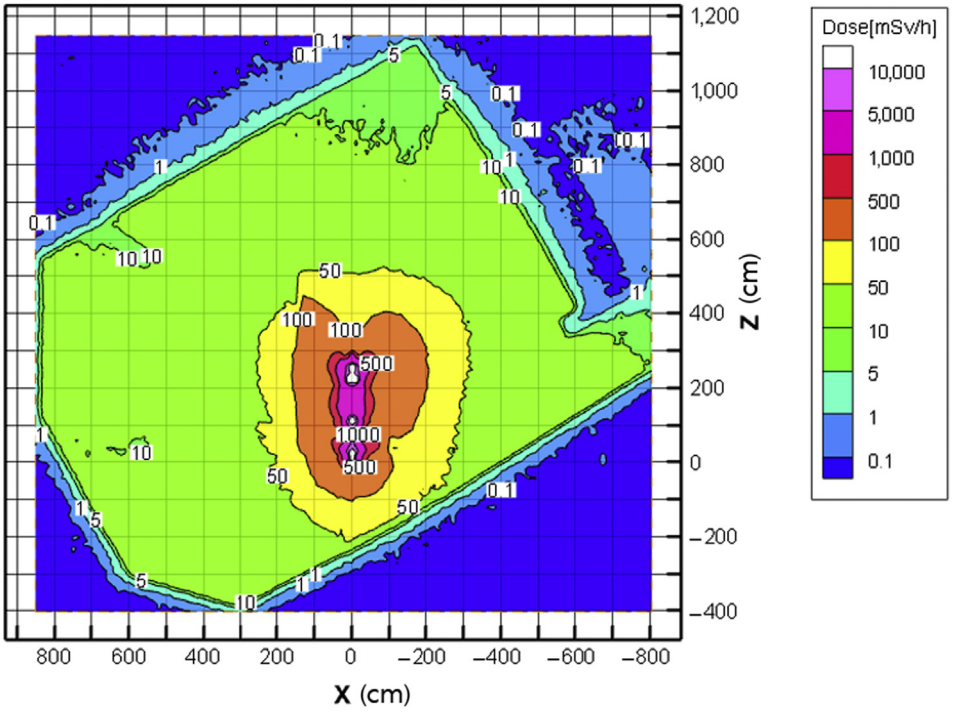

Fig. 6 – Neutron dose distribution in the treatment room. The image has been rotated clockwise by 60° from the general scheme shown in Fig. 2. The numbers on the contour line indicate the neutron dose level in millisieverts per hour. The cell size of the grid in this figure is 100 cm by 100 cm.

Table 4 – Neutron dose distribution near the target position.

Axial distance (cm)	Neutron equivalent dose per 1 Gy proton (mSv/Gy)				
	Lateral distance (cm)				
	0	50	100	150	200
0	7.513 ± 0.036	2.656 ± 0.019	1.368 ± 0.014	0.540 ± 0.008	0.350 ± 0.007
50	0.560 ± 0.008	0.988 ± 0.011	1.033 ± 0.012	0.439 ± 0.008	0.331 ± 0.007
100	0.382 ± 0.007	0.530 ± 0.008	0.676 ± 0.009	0.327 ± 0.007	0.271 ± 0.006
150	0.326 ± 0.006	0.402 ± 0.007	0.484 ± 0.008	0.230 ± 0.005	0.230 ± 0.005
200	0.313 ± 0.006	0.335 ± 0.006	0.401 ± 0.007	0.185 ± 0.005	0.203 ± 0.005

Table 5 – Neutron doses at various angles with constant radius (R = 15 cm, 50 cm, 100 cm, and 150 cm) from the target in millisieverts per 1 Gy proton absorbed dose.

Distance (cm)	Angle from beam axis			
	0°	45°	90°	135°
15	1.787 ± 0.018	1.683 ± 0.016	2.525 ± 0.020	5.559 ± 0.029
50	0.560 ± 0.008	1.044 ± 0.012	2.656 ± 0.019	7.123 ± 0.032
100	0.382 ± 0.007	0.846 ± 0.011	1.368 ± 0.014	1.646 ± 0.015
150	0.326 ± 0.006	0.656 ± 0.009	0.540 ± 0.008	1.218 ± 0.013

0.32 ± 0.01 mSv/Gy (simulation) and 0.21 ± 0.02 mSv/Gy (measurement) at the furthermost position (#8, 150 cm distance along the beam axis from the target).

4. Discussion

Fig. 9 provides a graphical comparison of the data at log scale. The simulation data in this study were used in the comparison, and the neutron dose equivalent was found to decrease from 4.942 ± 0.031 mSv/Gy to 0.324 ± 0.006 mSv/Gy as the distance increased from 0 cm (field edge) to 150 cm along the beam axis.

Yan et al's [10] measurement results at the Harvard Cyclotron Laboratory were 0.32 mSv/Gy at 46 cm, 0.24 mSv/Gy at 59 cm, and 0.1 mSv/Gy at 118 cm. These values are at most 72% lower than our results, but considering the low proton energy (160 MeV) and the fact that they used an unmodulated proton beam, the results are comparable. Another set of data was reported by Wroe et al [15] at the Loma Linda University Medical Center. Under the measurement conditions of 225 MeV proton beams with 8-cm and 13-cm apertures, the dose equivalent reportedly decreased from 3.9 mSv/Gy to 0.18 mSv/Gy as the lateral distance from the proton field edge increased from 2.5 cm to 60 cm. The upper graph in Fig. 8 for the 8-cm aperture shows a shape that is close to ours; this is because the results were obtained under similar conditions for beam energy and opening. Mesoloras et al's [13] findings are also

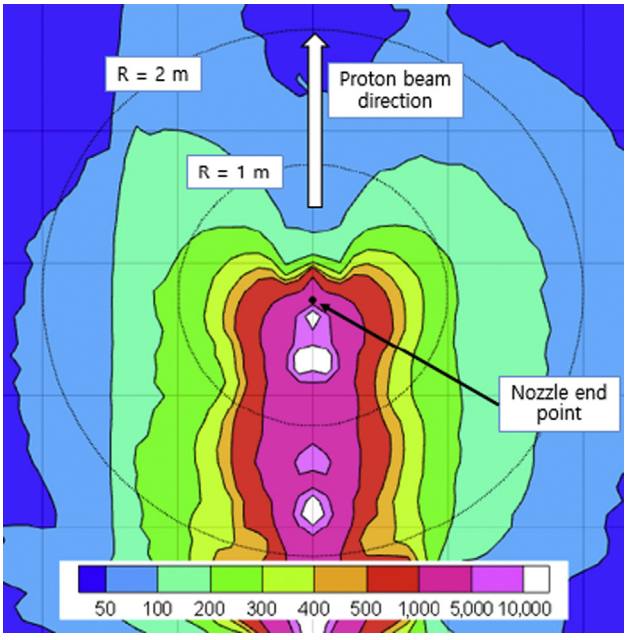

Fig. 7 – Neutron dose distribution in millisieverts at constant radius (R= 100 cm, 200 cm) from the target. Proton beam direction is parallel to Z axis in Fig. 6.

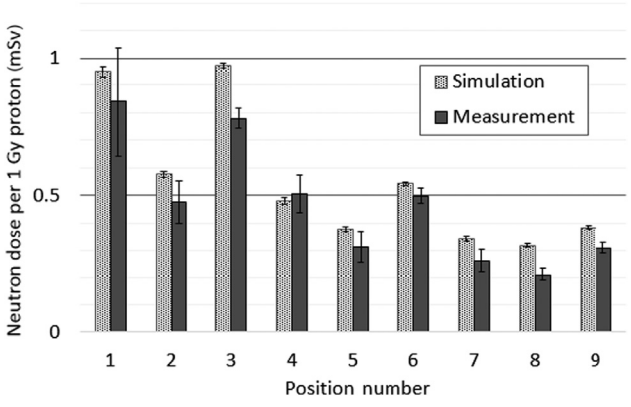

Fig. 8 – Comparison between measured and simulated data. Neutron dose equivalents were measured with ^{3}He neutron detector. Simulation data were acquired via interpolation from dose profile in Fig. 6. Position number is the same as in Fig. 3.

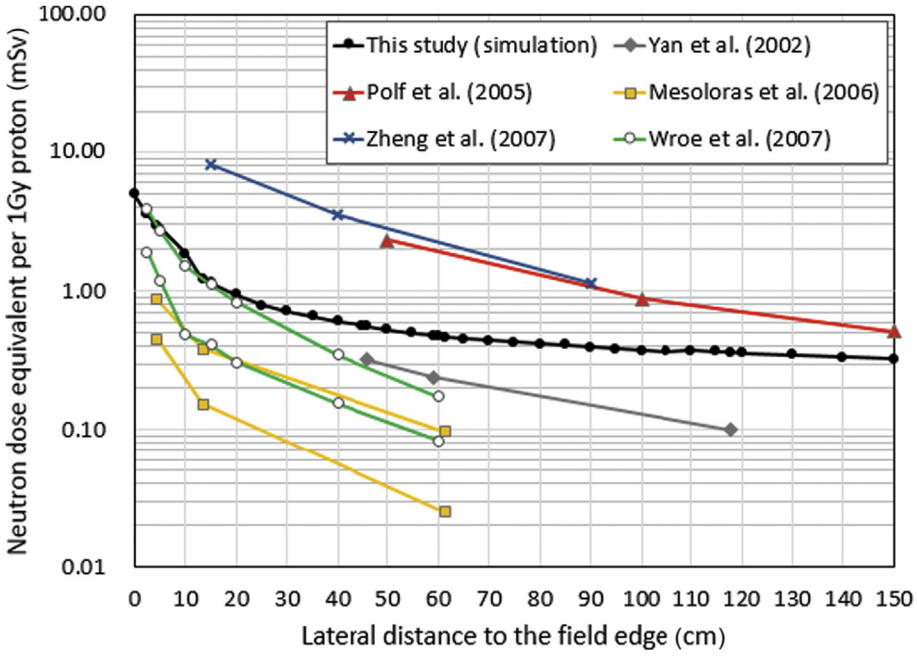

Fig. 9 – Comparison of neutron dose value. In this study, the data of Yan et al [10] and Zheng et al [16] were from Monte Carlo simulations, but the other data were obtained by measurement. Wroe et al [15] reported two sets of data: the upper plot is for an 8-cm aperture, and the lower for a 13-cm aperture. Mesoloras et al [13] reported two sets of data: the upper plot was for a 134-MeV proton beam with a 10-cm snout and lower for 119 MeV with a 13-cm snout.

comparable. They reported neutron dose equivalent data ranging from 0.03 mSv/Gy to 0.87 mSv/Gy, obtained from two different settings (10 cm snout for 134 MeV and 20 cm snout for 119 MeV). These results are 70% to 90% lower than our results, but are not deemed to indicate a major difference considering that that group used lower proton energy and larger beam openings.

Two published sets of Monte Carlo simulation data were compared. Polf and Newhauser's [12] MCNPX simulation results at the Harvard Cyclotron Laboratory show a decrease in the neutron dose from 150 cm along the beam axis. The maximum energy (2.3 mSv/Gy to 0.51 mSv/Gy when the distance from the field center was increased from 50 cm to 158 MeV) was lower than that in our study, but range modulation was applied up to 15 cm. The range modulation was three times higher than ours (5 cm), and it may be possible to generate more neutrons. The other study was conducted by Zheng et al [16], who modeled the M.D. Anderson Cancer Center proton nozzle with 250 MeV proton energy. They found that the neutron dose decreased from about 8 mSv/Gy to 1 mSv/Gy, proportionate to the distance from 15 cm to 90 cm along the beam axis. We found that these differences were relatively higher than was the case for other results, but the overall data trends were similar and the maximum difference was within 1 order of magnitude.

From the above results, we were able to identify that the secondary neutron dose during the proton therapy process is much too high. Moreover, the dose level is likely to reach over the safety level (100 mSv). For example, if the treatment plan involves using a 72-Gy proton beam (general case for gross volume treatments), the expected neutron dose will be approximately 355.68 mSv to 23.04 mSv at the patient position.

Through this study, it was possible to better understand the secondary neutron influence and distribution in the treatment space based on quantitative assessment. However, there are several limitations. First, there is a need to consider a greater number of nozzle settings. Although the theoretical background is the same, secondary particle generation is affected by the nozzle settings such as beam energy, scatterer selection, range modulation, combination of snout, aperture, and other factors. Thus, more analyses of the neutron influence will have to be undertaken by obtaining results at various settings. Second, there is a need to apply an anatomical phantom. Although the beam nozzle was modeled precisely in this study, the target was a simply formed water phantom. This issue was not important in this study because the focus was on the neutron distribution in a treatment room; however, for future research involving organ dose assessments, for example, an anatomic phantom should be applied. These matters should be considered in future research.

5. Conclusion

The main interest of this study was to assess secondary neutron effective dose during proton therapy. Through detailed modeling and simulation, neutron dose profile data were acquired. The measurements obtained successfully supported the simulation results. The neutron doses were calculated in millisieverts per proton absorbed dose at the target, and were compared with the values reported in other studies. The results of our study (from 4.94 mSv/Gy at end of the field to 0.32 mSv/Gy at 150 cm axial distance) were shown to be consistent with the results of other studies. Also, there were two additional

findings. One was that the photon contribution was 0.8% on average; the other was that the dominant neutron sources could be verified through the neutron flux calculation.

Conflicts of interest

All authors have no conflicts of interest to declare.

REFERENCES

[1] Particle Therapy Co-Operative Group (PTCOG) statistics, Available from: http://www.ptcog.ch/index.php/facilities-in-operation.

[2] D.R. Olsen, Ø.S. Bruland, G. Frykholm, I.N. Norderhaug, Proton therapy – a systematic review of clinical effectiveness, Radiother. Oncol. 83 (2007) 123–132.

[3] X.G. Xu, B. Bednarz, H. Paganetti, A review of dosimetry studies on external-beam radiation treatment with respect to second cancer induction, Phys. Med. Biol. 53 (2008) R193–R241.

[4] C.Z. Jarlskog, H. Paganetti, Risk of developing second cancer from neutron dose in proton therapy as function of field characteristics, organ and patient age, Int. J. Radiat. Oncol. Biol. Phys. 72 (2008) 228–235.

[5] National Council on Radiation Protection & Measurements (NCRP), Radiation Protection for Particle Accelerator Facilities, NCRP Report 144, 2003.

[6] A.M. Koehler, R.J. Schneider, J.M. Sisterson, Flattening of proton dose distributions for large-field radiotherapy, Med. Phys. 4 (1977) 297–301.

[7] E. Grusell, A. Montelius, A. Brahme, G. Rikner, K. Russell, A general solution to charged particle beam flattening using an optimized dual-scattering-foil technique, with application to proton therapy beams, Phys. Med. Biol. 39 (1994) 2201–2216.

[8] Th. Haberer, W. Becher, D. Schardt, G. Kraft, Magnetic scanning system for heavy ion therapy, Nucl. Instrum. Methods Phys. Res. A330 (1993) 296–305.

[9] E. Pedroni, R. Bacher, H. Blattmann, T. Böhringer, A. Coray, A. Lomax, S. Lin, G. Munkel, S. Scheib, U. Schneider, A. Tourovsky, The 200-MeV proton therapy project at the Paul Scherrer Institute: conceptual design and practical realization, Med. Phys. 22 (1995) 37.

[10] X. Yan, U. Titt, A.M. Koehler, W.D. Newhauser, Measurement of neutron dose equivalent to proton therapy patients outside of the proton radiation field, Nucl. Instrum. Methods Phys. Res. A 476 (2002) 429–434.

[11] S.C. Roy, G.A. Sandison, Scattered neutron dose equivalent to a fetus from proton therapy of the mother, Radiat. Phys. Chem. 71 (2004) 997–998.

[12] J.C. Polf, W.D. Newhauser, Calculations of neutron dose equivalent exposures from range-modulated proton therapy beams, Phys. Med. Biol. 50 (2005) 3859–3873.

[13] G. Mesoloras, G.A. Sandison, R.D. Stewart, J.B. Farr, W.C. His, Neutron scattered dose equivalent to a fetus from proton radiotherapy of the mother, Med. Phys. 33 (2006) 2479.

[14] R. Tayama, Y. Fujita, M. Tadokoro, H. Fujimaki, T. Sakae, T. Terunuma, Measurement of neutron dose distribution for a passive scattering nozzle at the Proton Medical Research Center (PMRC), Nucl. Instrum. Methods Phys. Res. A 564 (2006) 532–536.

[15] A. Wroe, A. Rosenfeld, R. Schulte, Out-of-field dose equivalents delivered by proton therapy of prostate cancer, Med. Phys. 34 (2007) 3449.

[16] Y. Zheng, W. Newhauser, J. Fontenot, P. Taddei, R. Mohan, Monte Carlo study of neutron dose equivalent during passive scattering proton therapy, Phys. Med. Biol. 52 (2007) 4481–4496.

[17] Los Alamos National Laboratory (LANL), MCNP6 User's Manual Version 1.0, 2008.

[18] National Institute of Standard and Technology (NIST), PSTAR program, Available from: http://physics.nist.gov/PhysRefData/Star/Text/PSTAR.html.

[19] International Atomic Energy Agency (IAEA), Absorbed Dose Determination in External Beam Radiotherapy, Technical Reports Series no. 398, 2000.

[20] International Commission on Radiological Protection (ICRP), Conversion Coefficients for Use in Radiological Protection Against External Radiation, 74, ICRP Pub, 1997.

[21] R.H. Olsher, H.H. Hsu, A. Beverding, J.H. Kleck, W.H. Casson, D.G. Vasilik, R.T. Devine, WENDI: an improved neutron rem meter, Health Phys. 79 (2000) 170–181.